Long Range Effects in Topologically Defective Arm-Chair Graphene Nanoribbons

Enrique Louis , Guillermo Chiappe * , José A. Vergés , Emilio San-Fabián *

Posted Date: 15 December 2023

doi: 10.20944/preprints202312.1125.v1

Keywords: graphene; nano-ribbons; long range effects

Article

Long Range Effects in Topologically Defective Arm-Chair Graphene Nanoribbons

Enrique Louis[1,‡], Guillermo Chiappe [2,*,‡], José A. Vergés [3,‡] and Emilio San-Fabián [4,*,‡]

[1] Departamento de Física Aplicada, and IUMA, Universidad de Alicante, 03080 Alicante, Spain; enrique.louis@ua.es
[2] Departamento de Física Aplicada, and IUMA, Universidad de Alicante, 03080 Alicante, Spain; chiappe@ua.es
[3] Departamento de Teoría y Simulación de Materiales, Instituto de Ciencia de Materiales de Madrid (CSIC), Cantoblanco, 28049 Madrid, Spain; jav@icmm.csic.es
[4] Departamento de Química Física, and IUMA, Universidad de Alicante, 03080 Alicante, Spain; sanfa@ua.es
* Correspondence: chiappe@ua.es(G.C.);sanfa@ua.es(E.S.F.)
‡ These authors contributed equally to this work.

Abstract: The electronic structure of 7/9-AGNR superlattices with up to eight unit cells has been studied by means of state of the art DFT and a model Hamiltonian that follows two different approaches: Hubbard type (Hu) and including long range Coulomb interaction (PPP), solved in the mean field approximation. We show that 7/9 interfaces stabilizes non polarized solutions at the mean field level. Considering non-polarized solutions, Hu and PPP Hamiltonians gives solutions with a gap that is closed as the size is increased. This is in line with DFT results. However the density of states around the Fermi level is not correctly described neither in Hu nor in the PPP model. We also interpret the DFT density of states in terms of bands of topological states: localized edge topological states and extended bulk topological states which interacts between them due to the long range Coulomb terms of Hamiltonian. In this line, we show that a screened long range interaction instead describe correctly DFT results and the interaction between topological states. Screening consists of introducing a parameter for an exponential decay in the long range potential of the model Hamiltonian, to vary its spatial range. Calculations on the superlattice just mentioned, illustrate the relevance of include appropriate long range interactions in determining the density of states around the Fermi level (Dirac point).

Keywords: graphene; nano-ribbons; long range effects

1. Introduction

Since its rediscovery in 2004, isolation and investigation by a Manchester team (very particularly by A.K. Geim and K.S. Novoselov, see Refs. [1,2]) graphene is offering to physicists and chemists an ever larger and richer field where to test the body of knowledge developed by researchers during the last one hundred years. Graphene, besides the expectations regarding fantastic technological applications, is defying the community of condensed matter physicists up to limits by no means anticipated [3]. Almost all experimental and theoretical tools developed in that period are finding a place in the flourishing field of graphene. Starting from its amazing Dirac character at energies near the Fermi level, the novel superconductivity observed in twisted bi-layers [3,4] along with zero-width bands which suggests the high relevance of electron-electron interaction in defining what points to be a non-BCS superconductivity, as in high temperature superconductors.

Meanwhile, richer physics has been predicted in twisted bi-layers. Collective excitations are a network of chiral edge plasmons entirely composed of excitations in the topological electronic edge states appear at AB-BA interfaces (See ref. [3]). Magic-angle twisted bilayer graphene (MATBG) exhibits a rich variety of electronic states, including correlated insulators, superconductors, and topological phases. Understanding the microscopic mechanisms responsible for these phases requires determining

Preprints (www.preprints.org) | NOT PEER-REVIEWED | Posted: 15 December 2023 doi:10.20944/preprints202312.1125.v1

the interplay between electron-electron interactions and quantum degeneracy due to spin and valley degrees of freedom. Signatures of strong electron-electron correlation have been observed at partial fillings of the flat electronic bands in recent spectroscopic measurements. Transport experiments have shown changes in the Landau level degeneracy at fillings corresponding to an integer number of electrons per moiré unit cell. However, the interplay between interaction effects and the degeneracy of the system is currently unclear. Using high-resolution scanning tunneling microscopy (STM), a cascade of transitions in the spectroscopic properties of MATBG as a function of electron filling, has been observed.

Changes in the chemical potential and a rearrangement of the low-energy excitations at each integer filling of the moiré flat bands are being identified. These spectroscopic features are a direct consequence of Coulomb interactions, which split the degenerate flat bands into Hubbard sub-bands. The cascade of transitions reported up to now characterizes the correlated high-temperature parent phase from which various insulating and superconducting ground-state phases emerge at low temperatures in MATBG. After the discovery of these astonishing effects in twisted layered samples, extraordinary experimental and theoretical efforts are being addressed to characterize the samples trying to find out how this amazing behavior depends on filling, the number of layers and the twisting angle, the three variables that seem to be crucial. The story, however, seems to be at the beginning, as recent experimental work clearly indicates that there is no need to twist the layered sample[3] to produce the superconductivity and other amazing effects similar to those observed in twisted samples.

In 2017 researchers of the University of Berkeley reported their findings of Topological states in junctions of arm-chair graphene nanoribons (AGNR) of different width [5]. Combining theoretical analyses with already developed bottoms-up techniques they were able to produce and characterize graphene samples with and without topological defects. Taking as unit cell the junction 7/9-AGNR, they studied various configurations ranging from an isolated 7-9 up to an infinite linear arrangement of 7-9 units (See Figure 1). They chose the 7-9 unit because one of the two possible ways to join the two ribbons (7 and 9) hosts an electronic topological state.

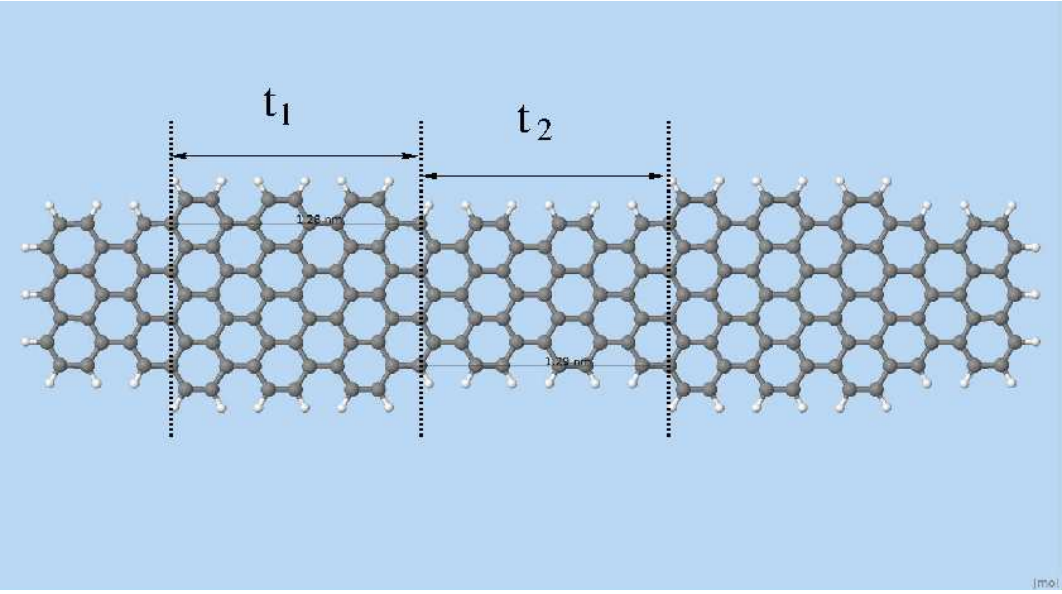

Figure 1. Schematic representation of the 7/9-AGNR with 2 unit cells (C2).

2. Method

In this work we focus on the effects of long-range interactions on the coupling between edge states in AGNRs superlattices (those mentioned in the previous paragraph). In particular, we consider finite 7/9-AGNR superlattices that are known to show topological defects at each 7-9 interface. The Hamiltonians we shall use are the *ab initio* DFT and the Pariser, Parr and Pople (PPP) [6,7]. Both,

Preprints (www.preprints.org) | NOT PEER-REVIEWED | Posted: 15 December 2023 doi:10.20944/preprints202312.1125.v1

spreadly used methods, incorporate short and long range electron-electron interaction and were handled within the restricted or unrestricted approximations that have been intensively applied to investigate the electronic structure of polycyclic aromatic hydrocarbon (PAH) [8].

Most DFT calculations were carried out using the B3LYP exchange-correlation functional[9–12], and the basis set 6-31G*[13,14], using the Gaussian-16 package[15]. All geometries have been optimized at B3LYP/6-31G* level. In order to obtain the polarised solutions, we work with the unrestricted approximation of both methods. The densities of states (DOS), were calculated by adding to the energy an imaginary part of 0.05 eV, independent of size, energy or whatever was calculated either by means of Green functions (PPP) or with Gaussian-16 and with the help of GausSum[16] and Multiwfn[17] programs. The PPP model Hamiltonian contains, besides the standard kinetic energy, both local on-site and long-range Coulomb interactions and a single π orbital per carbon atom. The non-interacting term incorporates two standard parameters, the orbital energy ϵ_0 and the hopping between nearest neighbor pairs t_{ij}, namely,

$$\hat{H}_0 = \epsilon_0 \sum_{i=1,N;\sigma} \hat{c}^{\dagger}_{i\sigma}\hat{c}_{i\sigma} + \sum_{<ij>;\sigma} t_{ij}\hat{c}^{\dagger}_{i\sigma}\hat{c}_{j\sigma} \ , \tag{1}$$

where the operator $\hat{c}^{\dagger}_{i\sigma}$ creates an electron at site i with spin σ, N is the number of orbitals and t_{ij} is the hopping between nearest neighbor pairs $<ij>$.

In cases where the distance d_{ij} between nearest neighbors pairs significantly deviates from standard value, $d_0 = 1.41$ Å, due, for instance, to defects or impurities, the hopping parameter may be scaled using the following scaling law adequate for π orbital [18] namely,

$$t_{ij} = \left(\frac{d_0}{d_{ij}}\right)^3 . \tag{2}$$

As regards the values of the model parameters we use the well-tested set reported in ref. [[19]].

Within the Hartree-Fock approximation (HF), the interacting term of the PPP Hamiltonian is approximated by,

$$\begin{aligned}\hat{H}^{HF}_{I-PPP} = U \sum_{i=1,N;\sigma} \left(\hat{n}_{i\sigma}\langle\hat{n}_{i\bar{\sigma}}\rangle - \frac{1}{2}\langle\hat{n}_{i\sigma}\rangle\langle\hat{n}_{i\bar{\sigma}}\rangle\right) \\ -\frac{1}{2}\sum_{i\neq j} V_{ij}\left(\langle\hat{n}_i\rangle\langle\hat{n}_j\rangle - \sum_{\sigma}\langle\hat{c}^{\dagger}_{i\sigma}\hat{c}_{j\sigma}\rangle\langle\hat{c}^{\dagger}_{i\sigma}\hat{c}_{j\sigma}\rangle - 1\right) \\ + \sum_{i\neq j} V_{ij}\left(\hat{n}_i\langle\hat{n}_j\rangle - \sum_{\sigma}\hat{c}^{\dagger}_{i\sigma}\hat{c}_{j\sigma}\langle\hat{c}^{\dagger}_{i\sigma}\hat{c}_{j\sigma}\rangle\right) .\end{aligned} \tag{3}$$

Here $\hat{n}_i = \sum_{\sigma}\hat{n}_{i\sigma}$ and $\hat{n}_{i\sigma}$ is the occupation number in the site i with spin σ. The first line of this equation is the HF version of the Hubbard Hamiltonian (Hu), which only retains local interactions. It is interesting to note the presence of non-diagonal terms in the third parenthesis of the last equation. These terms introduce frustration in non-frustrated lattices. This is surely the reason why the staggered polarization in the polarised configuration is always smaller in the PPP than in the Hu model.

In incorporating the interaction V_{ij} in the PPP model, one may choose the unscreened Coulomb interaction [20] although it is a common practice the use of interpolating formulae. In the case of polycyclic aromatic hydrocarbons (PAHs), that proposed by Ohno [21] has wide acceptance. We use that formula, modified to incorporate a parameter λ that allows to control the extent of the long range interactions. When $\frac{1}{\lambda} \to 0$ the unscreened Coulomb interaction is recovered.

$$V_{ij} = Ue^{-\frac{d_{ij}}{\lambda}}\left[1 + \left(\frac{Ud_{ij}}{e^2}\right)^2\right]^{-1/2} \tag{4}$$

Preprints (www.preprints.org) | NOT PEER-REVIEWED | Posted: 15 December 2023 doi:10.20944/preprints202312.1125.v1

where $U = 8.36\,eV$, d_{ij} is the distance between i and j atoms, in Angstroms and e is the electron charge. The parameter λ will be fixed in order to better reproduce with the PPP model the results obtained with *ab initio* DFT.

Supercells containing 1 (the unit cell is half the structure shown in Figure 1) 2, 4, 6 and 8 unit cells were in most cases used to illustrate the results. Other geometries were occasionally used to reinforce a given argument. Geometries were optimised with restricted DFT, at the B3LYP/6-31G* level. Optimised geometries do not differ much from the bulk geometry of graphene and very slightly depend on number of cells considered as can be seen in Table 1.

Table 1. Geometrical structure of 7/9-AGNR superlattice with 2, 3, 4, 6 and 8 (Cn)) unit cells calculated by means of DFT. In addition, results for the energies of HOMO and LUMO (in hartrees) and the Gap (in eV), are reported.

	C2: 192 C's	C3: 288 C's	NC4: 384 C's	C6: 576 C's	C8: 768 C's
t_1 (nm)	1.285	1.284	1.284	1.284	1.284
t_2 (nm)	1.295	1.293	1.293	1.293	1.293
ε_{HOMO}	-0.13783	-0.1333	-0.13234	-0.13198	-0.13187
ε_{LUMO}	-0.12441	-0.1294	-0.13065	-0.13112	-0.13126
Gap	0.365	0.107	0.046	0.023	0.017

3. Calculations and Results

The influence of a particular combination of exchange-correlation functional/basis set was investigated on all possible combinations of functionals B3LYP and PBEPBE[22] with the basis sets 6-311G*[23] and 6-31G*. The results are shown in Table 2.

Table 2. Several properties of 7/9-AGNR superlattice C2, calculated by means of DFT, using several methods and basis sets. All the energies are in hartree, except the Gap which is in eV. For t_1 and t_2, see the Figure 1

	B3LYP/6-31G*	PBE/6-31G*	B3LYP/6-311G*	PBE/6-311G*
t_1 (nm)	1.2845	1.2803	1.2828	1.2784
t_2 (nm)	1.2947	1.2903	1.2929	1.2883
ε_{HOMO}	-0.13783	-0.14419	-0.14661	-0.15097
ε_{LUMO}	-0.12441	-0.12801	-0.13396	-0.13557
Gap	0.365	0.440	0.344	0.419
E_{SCF}	-7350.247114	-7342.011956	-7351.563136	-7343.186493

In the context of the present work the most interesting property is the forbidden gap. The results for four combinations of functional & basis set are all within the range 0.344-0.440 eV. For sure other sources of errors are more important that this difference. Therefore, DFT calculations carried out in this work have been done with the B3LYP/6-31G* methods.

The influence of the polarized and non-polarized solutions, as well as the variation of the gap when the 7/9 interface is considered or not, has been analized for the case of two unit cells or their equivalents without interfaces (7/7 and 9/9). The Table 3 shows the results.

It is obvious that our calculations indicate that polarized solutions are more stable (see Table 3) but the difference in stability with the non-polarized is much smaller when the topological defect (7/9 interfaces) is present. This suggests that topological defects tend to stabilize non-polarized solutions. Furthermore polarized solutions in general exhibit larger gaps due to an overestimation of exchange in the mean field solutions. Therefore, hereafter we shall study non-polarized solutions using DFT, when the number of cells is increased. Likewise, the defect-free polarized solutions show a much larger gap than the polarized 7/9-AGNR, and while the non-polarized solutions of the 7/7 and 9/9 show hardly any gap, the non-polarized 7/9-AGNR shows a moderate gap (see Table 3). However we will show below that this gap closes when the size is increased.

Preprints (www.preprints.org) | NOT PEER-REVIEWED | Posted: 15 December 2023 doi:10.20944/preprints202312.1125.v1

Table 3. Forbidden gap of ribbon C2 with and without polarisation. The calculations were carried out with B3LYP/6-31G* and the geometry of the non-polarised AGNR. For the sake of comparison, results for the ribbon without topological defect are also shown. Fig 3 supports this conclusion: the solution including polarization clearly increases the gap (from 0.365 up to 0.836) while it does not affect overall polarization.

	7/9-AGRN		Without defect 7/7		Without defect 9/9	
	Non-Polarized	Polarized	Non-Polarized	Polarized	Non-Polarized	Polarized
E_{B3LYP}	-7350.24711	-7350.25368	-6435.41973	-6435.44606	-8266.25259	-8266.28214
ε_{homo} (E_h)	-0.13783	-0.14645	-0.13097	-0.15643	-0.13254	-0.16135
ε_{lumo} (E_h)	-0.12441	-0.11571	-0.12859	-0.10275	-0.13032	-0.10104
Gap (eV)	0.365	0.836	0.065	1.460	0.060	1.640
$\Delta E_{Pol-NoPol}$	0.0066		0.0263		0.0295	

Figure 2 shows the total density of states (TDOS) in a sufficiently wide range of energies (referred to the Fermi level) for ribbons with 2, 4 and 8 unit cells. The figure provides a rather pictorial summary of the superstructures we shall be dealing with in this work. The most interesting energy region lies in the range (-2, 2) eV. Inside that region all contributions of topological and edge states are found. The changes in the TDOS as the size of the supercell increases are noticeable, particularly around the Fermi level which is taken as zero energy in the plot.

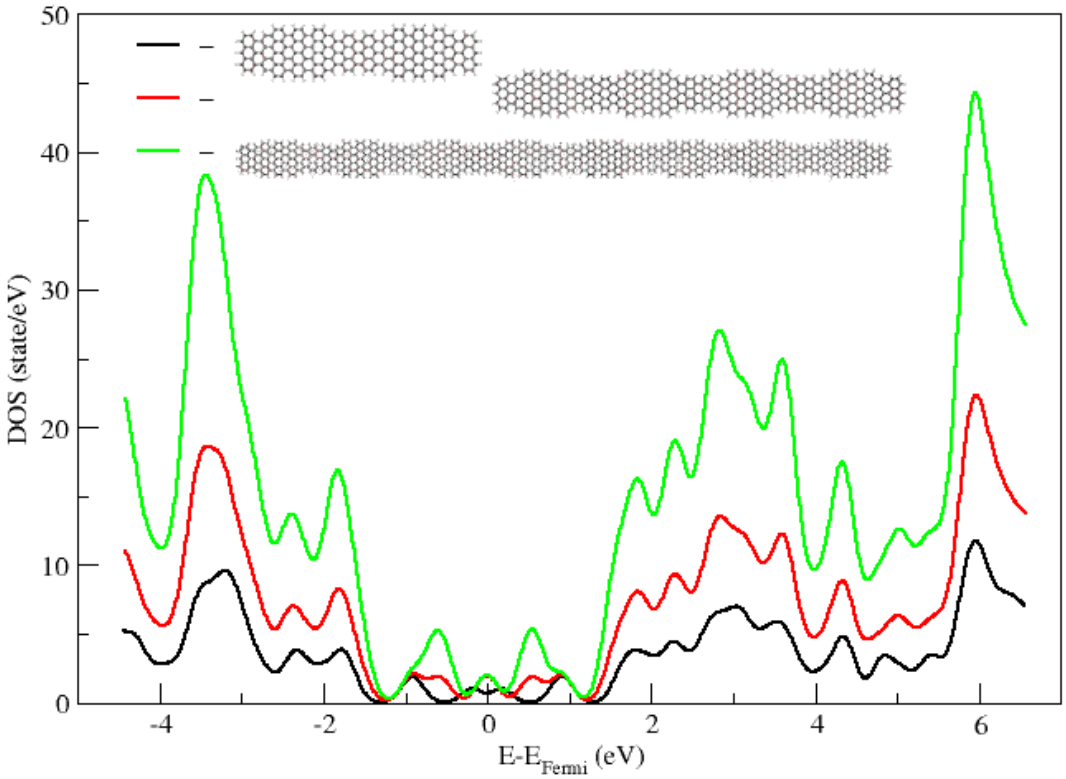

Figure 2. Total density of states in 7/9-AGNR superlattices with 2, 4 and 8 unit cells calculated by means of DFT method, in the energy range (-5,7). Edge and topological states lie in the region -1 up to 1 eV (energy refereed to the Fermi level).

In order to better identify these changes and its origin, we also calculate the partial density of states (PDOS). Figure 3 shows PDOS for all superstructures C1 to C8. Partial densities of states

Preprints (www.preprints.org) | NOT PEER-REVIEWED | Posted: 15 December 2023 doi:10.20944/preprints202312.1125.v1

for different C's were obtained by adding up local density of states of layers with 96 atoms and its symmetrical in the sample (1-96, ..., 289-384). Therefore in the case of C1 and C2 these PDOS are the total density of states.

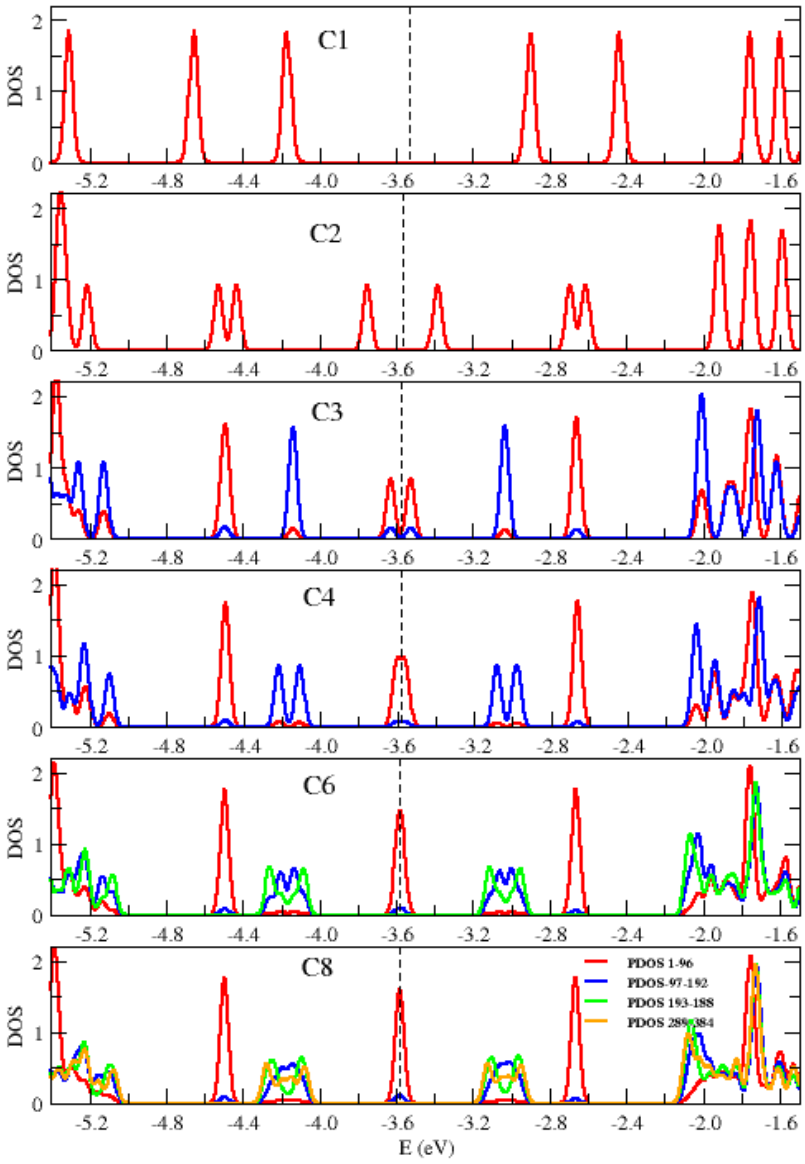

Figure 3. Total density of states in 7/9-AGNR superlattices with 1- 8 (C1-C8) unit cells calculated by means of B3LYP/6-31G* method. Partial densities of states (PDOS) were obtained by adding up local density of states on symmetrical Cs in contiguous layers of 96 atoms (1-96, ..., 289-384). The case (1-96, red continuous curve) corresponds to an unit cell, and thus is the only one without weight in the energy regions where topological states show up, around -1.5 and -5.4 eV (the Fermi level is approximately at -3.6 eV).

It is worth discussing in detail how the DOS around the Fermi level evolves with size. To this end we will show that a model states localized around 7/9 frontiers 7/9 (topological states) allows to give a description which is qualitatively right. We start with the smallest superstructure C1. Although it is a very special one, because of the very large effect of edges, it is useful to describe it within the kind of ideas that which will later be used to analyze larger sizes. A unit cell contains two 7/9 frontiers and two edges. There are four states, two coming from the edge states, and two from states localized at

Preprints (www.preprints.org) | NOT PEER-REVIEWED | Posted: 15 December 2023 doi:10.20944/preprints202312.1125.v1

the frontiers, which split by interactions amongst them due to the long range term of the Coulomb interaction, raising the four peaks seeing in the first panel of Figure 3. Two peaks correspond to states more localized at edges (the more symmetrically separated around the Fermi level) and two more localized around the 7/9 interfaces and close to the Fermi level. This is similar to the description of the states of a four sites first neighbors tight-binding open chain.

We apply these ideas to analyze C2. This superstructure has two unit cells, each one with two topological states, and each one now brings only one edge state. So we have six states that split into pairs below and above the Fermi level. The pair of peaks far away the Fermi level correspond to states more localized at edges of the sample so we call them edge states. Next there are two pairs of peaks, the first corresponding to states more localized at the first 7/9 frontier and the pair of states closer to the Fermi level correspond to states localized around the two more internal frontiers of C2. It is also similar to the description of states in a six sites open chain. The structure of peaks (red peaks in all panels) that raises from it will stay for larger samples. In larger samples it represent the DOS corresponding to the edge units of the sample. But the edge units will become less interacting as the sample becomes more larger, then the peaks associated with its evolve to a three peaks structure, doubly degenerated, one at the Fermi level and two additional peaks, one below and another above it, like two isolated three sites open chain. We suggest that these peaks correspond to topological edge states. From C3 to C8 the peak feature around -4.5 and -2.6 eV can be separated in pieces by the location of the states in the sample, following the same ideas. For C3 we have three unit cells. Therefore we will see two edge units, that provide the red peaks. In addition we have two topological states in the central unit, which gives the blue peaks. These two states are split by interactions between them and with edge units. We call these states topological bulk states. See Figure 4 For C4, the peaks coming from the edge units close to the Fermi level are already merged in only one peak at the Fermi level because the weakness of the interaction they suffer. And therefore it will be so for larger strips. Now we have four topological bulk states at the two central units. This four topological bulk states can be described like a two sites chain, and each site representing a unit with two interacting levels (see Figure 4) . This correspond to the four split blue peaks around the Fermi level. For C6 and C8 the analysis follow the same way. The edge states, red lines, remain quasi unchanged in C6 (C8). Now we have more central units that can be model like a tight-binding chain with two level sites that provide peaks blue, green and orange.

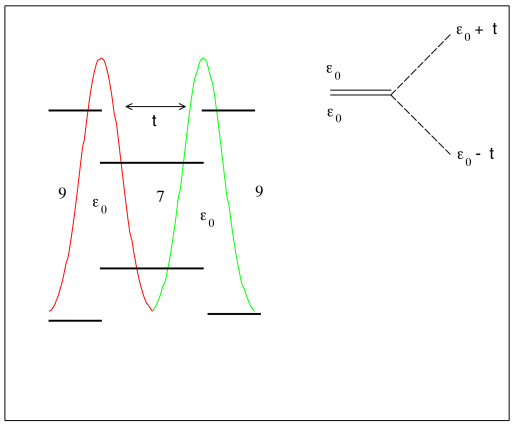

Figure 4. Schematic representation of topological bulk sates localized at the internal boundaries of a unit cell in the bulk. When connected it can be modeled like a chain with a two levels unit cell.

Preprints (www.preprints.org) | NOT PEER-REVIEWED | Posted: 15 December 2023 doi:10.20944/preprints202312.1125.v1

The picture raising after this study is that we have three flat bands corresponding to topological edge states, one just at, one below and one above the Fermi level (red lines in the figure), which would be model as a three initially degenerated level system at Fermi level with an effective coupling between them that breaks the degeneracy. In addition we have two broader bands, below and above the Fermi level, corresponding to topological bulk states. No gap is present in the system.

To end this discussion it is interesting to show how are the molecular orbitals in the energy window analyzed and how it is related with the discussion of Figure 3. We choose superstructure C4 to do this. Results for the four homo of highest energy in C4 are depicted in Figure 5. The state with the lowest energy (N-3) is clearly an edge state, like the state with the large energy, corresponding to red peaks . The next two states are associated to the topological bulk states corresponding to the blues peaks.

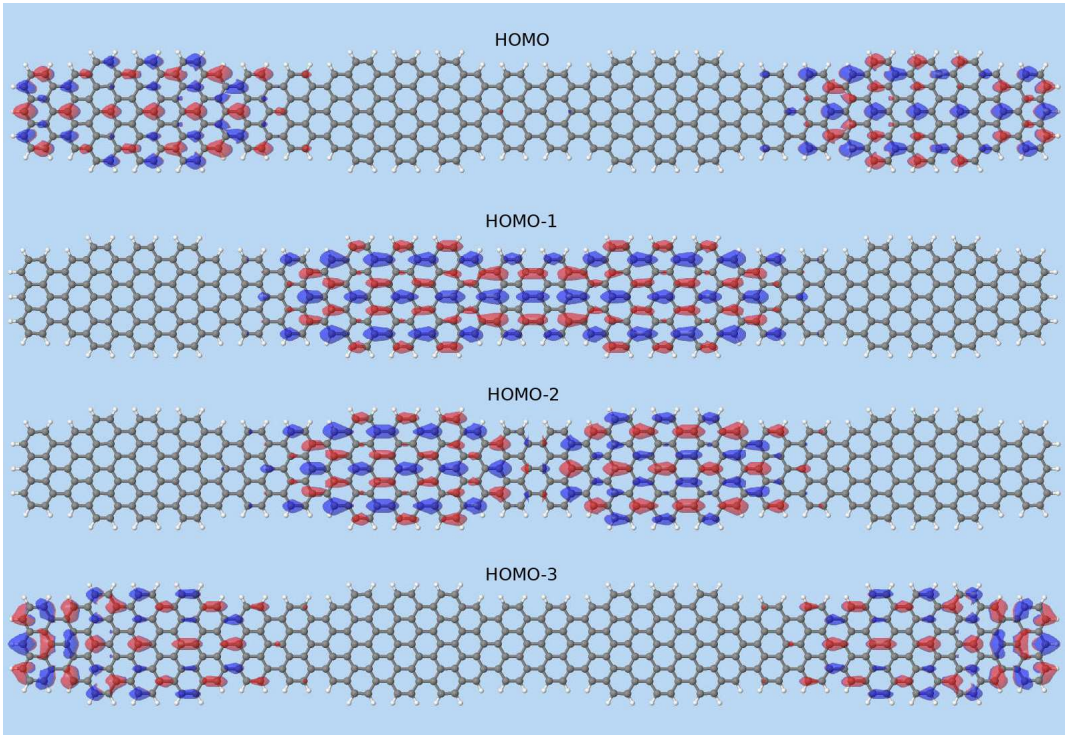

Figure 5. The highest molecular orbitals occupied for the superlattice with 4 unit cells.

Table 4 and Figure 6 shows the forbidden gap obtained with PPP. We include, for completeness, results for polarized solutions also, but we will focus finally in the non-polarized solutions. We use the PPP hamiltonian without screening (non local interaction, NL), and the Hubbard Hamiltonian (local interaction, L). The the most remarkable features of these calculations are: i) With local interaction and non polarized solutions we obtain a small gap for any size, which is apparently in line with DFT results. ii) With non local interaction the gap is slightly larger, but also tends to 0 with the size of the system. iii) Polarized solutions show a large gap in any case.

It is interesting to wonder if this picture can be reproduced by the PPP model, mainly concerning to the gap in the DOS.

Preprints (www.preprints.org) | NOT PEER-REVIEWED | Posted: 15 December 2023 doi:10.20944/preprints202312.1125.v1

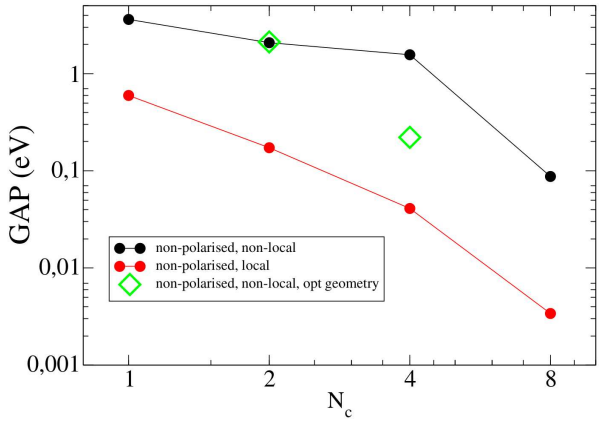

Figure 6. Forbidden gap of 7/9-AGNR superlattice vs the number of unit cells C1, C2, C4, C8. The results correspond to unrestricted non-polarised solutions of the PPP Hamiltonian including or not the long-range interaction (black and red circles, respectively) using a standard non optimized geometry for the superlattice. Some results obtained by using the DFT optimized geometry of previous calculations (green rhombus) are also shown.

Apparently L or NL interactions, both leads to zero gap for non polarized solutions as the size is increased. However comparing in detail with DFT solutions discrepancies arise. It is is shown in Figure 7. It shows the variation of TDOS, for the cases of 2 and 4 unit cells, using the PPP formalism, and considering the non-local (red line) and local potential (black line) for C2 and C4 structures. Although L interaction gives correctly the DFT result at the Fermi level (a small gap for C2 and a peak for C4) around the Fermi level the description is not that similar because it has a larger density of states than DFT. For NL interaction we obtain a so much larger gap. Both facts are due to the incorrect representation of interaction between topological states coming from both models. Local interaction underestimate it and non local interaction overestimate it. To improve these results we use the $V_{i,j}$ screened potential, adjusting λ factor. We found that $\lambda = 2$ gets the results qualitatively similar to DFT (green line in the figure). This screened interaction potential seems to represent more accurately the physics of these strips.

Table 4. Forbidden gap of 7/9-AGNR superlattice containing 1, 2, 4 and 8 unit cells (N_c) (see Fig.1) as calculated by solving the PPP Hamiltonian within the unrestricted approximation. Calculations for polarised and non-polarised configurations were done. In addition, results obtained removing the non-local (NL) interaction term in eq. (4) are also shown. If instead, it is the local term the one removed, the gap is again independent of length albeit at a smaller value of 3.0 eV. All results in eV.

	Gap (eV)				E^{PPP}_{UHF} (eV)			
	Non-polarised		Polarised		Non-polarised		Polarised	
N_c	NL	L	NL	L	NL	L	NL	L
C1	3.616	0.597	*	4.893	-1037.562	-894.092	*	-906.222
C2	2.085	0.173	3.035	4.841	-2078.726	-1792.47	-2079.175	-1815.905
C4	1.567	0.041	2.970	4.824	-4161.08	-3589.361	-4162.539	-3635.361
C8	0.088	0.003	3.069	4.819	-8092.643	-7183.256	-8095.469	-7273.997

* Not converging

Preprints (www.preprints.org) | NOT PEER-REVIEWED | Posted: 15 December 2023 doi:10.20944/preprints202312.1125.v1

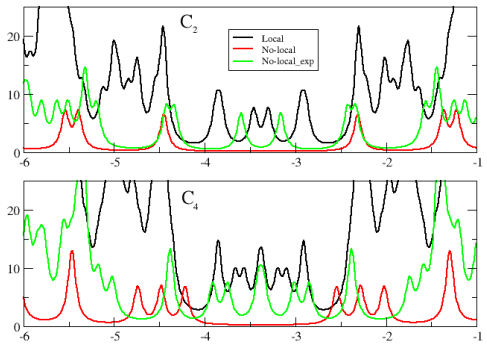

Figure 7. TDOS of 7/9-AGNR superlattice with 2 and 4 unit cells (C2 and C4), using the PPP model with only local potential (black line), with no-local potential (red line) and exponential screened non local interaction (green line).

4. Conclusions

The data presented in this work support the following conclusions and remarks:

1) We have shown that combining a model Hamiltonian (PPP) with DFT allows to identify the effects of short and long range interactions in 7/9-AGNR superlattices.
2) Topological defects at the 7/9 interfaces stabilize non-polarized against polarized solutions at the mean field level.
3) In order to vary the decay of the electron-electron interaction a exponentially modulated parameter can be used. It demonstrate to be necessary parameter to be included for improve the agreement between PPP and DFT solutions, particularly in what concerns to the description of DOS around the Fermi level.
4) We have given a plausible route for the evolution of the system density of states in going from the smallest C1 up to the largest superlattice C8.
5) In going through this route we have identified two types of localized states. One are topological edge states, which come from a combination of topological and edge states in the border units, which provides three flats bands, one at the Fermi level and two away from it, above and below. The others are topological bulk states which come from a tight binding model of two levels units cells. It provides two more width bands, below and above the Fermi level.

Author Contributions: Conceptualization, methodology, calculations and writiing, E.L., G.C., J.A.V. and E.S.F.. All authors have read and agreed to the published version of the manuscript.

Funding: This research was funded by the Spanish "Ministerio de Ciencia e Innovación" (grant PID2019-106114GB-I00), AICO/2021/093, PROMETEO/2021/017 ("Generalitat Valenciana") and the Universidad de Alicante.

Acknowledgments: Financial support by the Spanish "Ministerio de Ciencia e Innovación" (grant PID2019-106114GB-I00), AICO/2021/093, PROMETEO/2021/017 ("Generalitat Valenciana") and the Universidad de Alicante, is gratefully acknowledged. G.C. acknowledges a financial support from the Spanish Ministry of Education and Science, PID2019-109539GB-C41.

Conflicts of Interest: Declare conflicts of interest or state "The authors declare no conflict of interest."

References

1. Novoselov, K.S.; Geim, A.K.; Morozov, S.V.; Jiang, D.; Zhang, Y.; Dubonos, S.V.; Grigorieva, I.V.; Firsov, A.A. Electric Field Effect in Atomically Thin Carbon Films. *Science* **2004**, *306*, 666–669, [https://www.science.org/doi/pdf/10.1126/science.1102896]. https://doi.org/10.1126/science.1102896.

2. Meyer, J.; Geim, A.K.; Katsnelson, M. I.and Novoselov, K.S.; Booth, T.J.; Roth. The structure of suspended graphene sheets. *Nature* **2007**, *446*, 60–63. https://doi.org/10.1038/nature05545.
3. Guinea, F. https://doi.org/10.36471/JCCM_November_2021_01, 2021. Accesed:2023-12-07.
4. Cao, Y.; Fatemi, V.; Fang, S.; Watanabe, K.; Taniguchi, T.; Kaxiras, E.; Jarillo-Herrero, P. Unconventional superconductivity in magic-angle graphene superlattices. *Nature* **2018**, *556*, 43–50. https://doi.org/10.1038/nature26160.
5. Rizzo, D.J.; Veber, G.; Cao, T.; Bronner, C.; Chen, T.; Zhao, F.; Rodriguez, H.; Louie, S.G.; Crommie, M.F.; Fischer, F.R. Topological band engineering of graphene nanoribbons. *Nature* **2018**, *560*, 204–208. https://doi.org/10.1038/s41586-018-0376-8.
6. Pariser, R.; Parr, R.G. A Semi-Empirical Theory of the Electronic Spectra and Electronic Structure of Complex Unsaturated Molecules. I. *J. Chem. Phys.* **1953**, *21*, 466–471. https://doi.org/10.1063/1.1698929.
7. Pople, J.A. Electron interaction in unsaturated hydrocarbons. *Trans. Faraday Soc.* **1953**, *49*, 1375–1385. https://doi.org/10.1039/TF9534901375.
8. Chiappe, G.; Louis, E.; San-Fabián, E.; Vergés, J.A. Can model Hamiltonians describe the electron–electron interaction in π-conjugated systems?: PAH and graphene. *J. Phys.-Condens. Mat.* **2015**, *27*, 463001. https://doi.org/10.1088/0953-8984/27/46/463001.
9. Becke, A.D. Density-functional exchange-energy approximation with correct asymptotic behavior. *Phys. Rev. A* **1988**, *38*, 3098–3100. https://doi.org/10.1103/physreva.38.3098.
10. Lee, C.; Yang, W.; Parr, R.G. Development of the Colle-Salvetti correlation-energy formula into a functional of the electron density. *Phys. Rev. B* **1988**, *37*, 785–789. https://doi.org/10.1103/PhysRevB.37.785.
11. Becke, A.D. Density functional thermochemistry. III. The role of exact exchange. *J. Chem. Phys.* **1993**, *98*, 5648–5652, [http://aip.scitation.org/doi/pdf/10.1063/1.464913]. https://doi.org/10.1063/1.464913.
12. Stephens, P.J.; Devlin, F.J.; Chabalowski, C.F.; Frisch, M.J. Ab Initio Calculation of Vibrational Absorption and Circular Dichroism Spectra Using Density Functional Force Fields. *J. Phys. Chem.* **1994**, *98*, 11623–11627, [http://dx.doi.org/10.1021/j100096a001]. https://doi.org/10.1021/j100096a001.
13. Here, W.J.; Ditchfield, R.; Pople, J.A. Self-consistent molecular orbital methods XII. Further extensions of Gaussian-Type Basis sets for use in molecular orbital studies of organic molecules. *J. Chem. Phys.* **1972**, *56*, 2257. https://doi.org/10.1063/1.1677527.
14. Hariharan, P.C.; Pople, J.A. The influence of polarization functions on molecular orbital hidrogenation energies. *Theor. Chim. Acta* **1973**, *28*, 213. https://doi.org/10.1007/BF00533485.
15. Frisch, M.J.; Trucks, G.W.; Schlegel, H.B.; Scuseria, G.E.; Robb, M.A.; Cheeseman, J.R.; Scalmani, G.; Barone, V.; Petersson, G.A.; Nakatsuji, H.; et al. Gaussian 16 Revision C.01. https://gaussian.com/gaussian16, 2016. Gaussian Inc. Wallingford CT.
16. O'boyle, N.M.; Tenderholt, A.L.; Langner, K.M. cclib: A library for package-independent computational chemistry algorithms. *Journal of Computational Chemistry* **2008**, *29*, 839–845, [https://onlinelibrary.wiley.com/doi/pdf/10.1002/jcc.20823]. https://doi.org/https://doi.org/10.1002/jcc.20823.
17. Lu, T.; Chen, F. Multiwfn: A multifunctional wavefunction analyzer. *J. Comput. Chem.* **2012**, *33*, 580–592. https://doi.org/10.1002/jcc.22885.
18. Papaconstantopoulos, D.A., Ed. *Handbook of the Band Structure of Elemental Solids*; Springer, New York, MY, 2015. https://doi.org/10.1007/978-1-4419-8264-3.
19. Vergés, J.A.; Chiappe, G.; Louis, E. On the forbidden gap of finite graphene nanoribbons. *Eur. Phys. J. B* **2015**, *88*, 200. https://doi.org/10.1140/epjb/e2015-60389-5.
20. Mahan, G.D., Ed. *Many-Particle Physics (Physics of Solids and Liquids)*; Springer, Boston, MA, 2000. https://doi.org/10.1007/978-1-4757-5714-9_1.
21. Ohno, K. Some remarks on the Pariser-Parr-Pople method. *Theor. Chim. Acta* **1964**, *2*, 219–227. https://doi.org/10.1007/BF00528281.
22. Perdew, J.P.; Burke, K.; Ernzerhof, M. Erratum: Generalized Gradient Approximation Made Simple [Phys. Rev. Lett. **77**, 3865 (1996)]. *Phys. Rev. Lett.* **1997**, *78*, 1396–1396. https://doi.org/10.1103/PhysRevLett.78.1396.
23. Krishnan, R.; Binkley, J.S.; Seeger, R.; Pople, J.A. Self-consistent molecular orbital methods XX. A basis set for correlated wave functions. *J. Chem. Phys.* **1980**, *72*, 650. https://doi.org/10.1063/1.1677527.

 doi:10.20944/preprints202312.1125.v1